

Hadronic origin of the very high-energy gamma-ray emission from the low-luminosity AGN in NGC 4278

Asahi SHOJI,^{1,*} Yutaka FUJITA,¹ Norita KAWANAKA,¹ Susumu INOUE² and Kosuke NISHIWAKI³

¹Department of Physics, Graduate School of Science, Tokyo Metropolitan University
1-1 Minami-Osawa, Hachioji-shi, Tokyo 192-0397

²International Center for Hadron Astrophysics, Chiba University
1-33 Yayoi-cho, Inage-ku, Chiba City, Chiba 263-8522

³INAF Istituto di Radioastronomia, Via P. Gobetti 101, I-40129 Bologna, Italy

*E-mail: asasyo922@gmail.com

ORCID: 0009-0008-8373-2560, 0000-0003-0058-9719, 0000-0001-8181-7511, 0000-0003-1096-9424, 0000-0003-2370-0475

Abstract

The Large High Altitude Air Shower Observatory has detected very high-energy (VHE) gamma rays from NGC 4278, which is known to host a low-luminosity active galactic nucleus (AGN). Having only very weak radio jets, the origin of its VHE gamma rays is unclear. In this paper we first show that NGC 4278 has a massive molecular cloud surrounding the nucleus by analyzing data taken with the Atacama Large Millimeter/submillimeter Array. We then assume that cosmic ray protons are accelerated in a radiatively inefficient accretion flow around the supermassive black hole, which diffuse into the molecular cloud and produce gamma rays and neutrinos via pp interactions. We model the gamma-ray spectra and find that the observations can be explained by such hadronic processes if the AGN activity was higher in the past than at present, and the diffusion coefficient in the molecular cloud is appreciably smaller than in the Milky Way interstellar medium. However, we also show that the high-energy neutrinos co-produced with the gamma rays are unlikely to be detectable even with IceCube-Gen2.

Keywords: galaxies: individual (NGC 4278) — galaxies: nuclei — gamma rays: galaxies

1 Introduction

The detection of very high-energy (VHE) gamma rays from active galactic nuclei (AGN) provides crucial insights into the physical processes that occur in these extreme environments. Recently, the Large High Altitude Air Shower Observatory (LHAASO) reported the detection of TeV gamma rays from 1LHAASO J1219+2915 during 2021–2023 (Cao et al. 2024a; Cao et al. 2024b), which is spatially coincident with NGC 4278, an elliptical galaxy at a distance of $D_L = 16.1$ Mpc (Tonry et al. 2001). NGC 4278 harbors a supermassive black hole (SMBH) with a mass of $M_{\text{BH}} = (3.09 \pm 0.58) \times 10^8 M_\odot$ (Wang, & Zhang 2003; Chiaberge et al. 2005) and exhibits characteristics of a low-luminosity active galactic nucleus (LLAGN), with a small Eddington ratio¹ of $\dot{m} \sim 5 \times 10^{-6}$ (Younes et al. 2010; Hernández-García et al. 2014). This discovery is particularly intriguing because the AGN of NGC 4278 is observed to possess only a very weak jet, much less powerful than those for typical gamma-ray sources such as blazars or radio galaxies (Cao et al. 2024b). Previous studies have attempted to explain the gamma-ray emission during the active state through various jet-based models, including synchrotron self-Compton (SSC) (Lian et al. 2024; Dutta & Gupta 2024) and combined SSC + pp interactions (Wang et al. 2024), supported by the detection of two-sided symmetric jets on sub-parsec scales by VLBA observations (Giroletti et al. 2005). However, crucial properties such as the Doppler factor of the jet is unknown, and it is not obvious how the very weak radio jets can accelerate high-energy particles that can

produce the observed VHE gamma rays.

A separate noteworthy fact is that NGC 4278 is known to possess an exceptionally large amount of HI gas on scales of 30–40 kpc, with total mass $\sim 10^8 M_\odot$. This is unusually large for an elliptical galaxy (Raimond et al. 1981; Morganti et al. 2006; Haynes et al. 2018).

In this paper, we first show that NGC 4278 has a massive molecular cloud near its center by analyzing data from the Atacama Large Millimeter/submillimeter Array (ALMA). We then propose that the gamma-ray emission from NGC 4278 can be explained by the interaction between cosmic ray (CR) protons² accelerated by the AGN and those in the molecular cloud, similar to the model applied to the gamma-ray emission around Sagittarius A* (Sgr A* ; Fujita et al. 2015; Fujita et al. 2017). This mechanism is particularly attractive because NGC 4278, as an LLAGN, is likely to host a radiatively inefficient accretion flow (RIAF). These flows, which form at relatively low mass accretion rates ($\dot{m} \lesssim 0.1$ – 0.01), are characterized by strong turbulence that can potentially accelerate CR protons to PeV energies by stochastic acceleration (Kimura et al. 2015). The possible strong turbulence and magnetic fields within the molecular cloud may allow the CR protons to remain trapped and diffuse for a long time, possibly explaining the observed gamma-ray emission. The gamma-ray emission from NGC 4278 appears to show two distinct states: an active state and a quasi-quiet state, both detected by LHAASO. While Fermi-LAT has detected GeV gamma-ray emission corresponding to the active state (Bronzini et al. 2024), only upper limits were obtained

¹ The mass accretion rate normalized by the Eddington mass accretion rate. See equation (2).

² In this paper, CRs refer to CR protons unless otherwise noted.

during the quasi-quiet state (Abdollahi et al. 2022; Ballet et al. 2023; Lian et al. 2024). While the VHE gamma rays are variable, we focus mainly on the steady ones emitted during the quasi-quiet state.

We present our modeling of CR diffusion and the resulting gamma-ray emission from pp interactions within the molecular cloud. Our analysis focuses on determining whether this hadronic scenario can account for the observed gamma-ray spectrum during the quasi-quiet state. Additionally, we explore the implications of this model for potential neutrino detection by future instruments, which would provide definitive proof of the hadronic origin of the gamma-ray emission.

2 ALMA observation of NGC 4278

2.1 Data Reduction

NGC 4278 was observed with ALMA at the frequency of the CO($J=2-1$) rotational transition line (230.54 GHz at the rest frame; project code 2022.1.01173.S). The observation was performed with a single pointing, centered on the galaxy on March 9, 2023, with an exposure time of 34 minutes. The data were calibrated with the appropriate version of the Common Astronomy Software Application (CASA) software (McMullin et al. 2007) and the ALMA pipeline for quality assurance.

We subtracted the continuum emission using line-free channels with the CASA task `uvcontsub` (`fitorder = 1`) to study the line emissions. We reconstructed the line cubes and the underlying continuum maps with the CASA task `tclean` with a threshold of 3σ . We used natural weighting, following previous studies of elliptical galaxies (Olivares et al. 2019; Russell et al. 2019; Fujita et al. 2023; Fujita et al. 2024). The synthesized beam size is $7.1'' \times 6.3''$ and the rms in the final data cube is $\sim 9 \text{ mJy beam}^{-1}$.

The CASA task `imoments` was used to generate images of the integrated intensity, the intensity-weighted mean radial velocity, and the intensity-weighted mean velocity dispersion (full width at half maximum or FWHM). The results are shown in figure 1. The integrated intensity map in the left panel shows that the CO emission extends to the northeast on a scale of $\sim 150 \text{ pc}$. The velocity center distribution map in the middle panel suggests rotational motion around the AGN with velocities of $\sim 150\text{--}200 \text{ km s}^{-1}$. The axis of rotation is close to the direction of the inner radio jets (Giroletti et al. 2005).

2.2 Molecular Gas Mass

The CO intensity of the elongated cloud around the AGN (figure 1 left) is $S_{\text{CO}}\Delta v \approx 11 \text{ mJy beam}^{-1} \text{ km s}^{-1}$. We estimate the mass of the molecular gas from the intensity using the following relationship from Bolatto et al. (2013):

$$M_{\text{mol}} = \frac{1.05 \times 10^4}{F_{21}} \left(\frac{X_{\text{CO}}}{2 \times 10^{20} \frac{\text{cm}^{-2}}{\text{K km s}^{-1}}} \right) \left(\frac{1}{1+z} \right) \left(\frac{S_{\text{CO}}\Delta v}{\text{Jy km s}^{-1}} \right) \left(\frac{D_L}{\text{Mpc}} \right)^2 M_{\odot}, \quad (1)$$

where X_{CO} is the conversion factor from CO to H_2 and $D_L = 16.1 \text{ Mpc}$ is the luminosity distance to NGC 4278. The redshift of NGC 4278 is $z \sim 0$. We take $F_{21} = 3.2$ for the CO($J=2-1$)/CO($J=1-0$) line flux ratio, as assumed in other studies when this value is not directly measured. Since the conversion factor X_{CO} is not well understood for elliptical galaxies, we assume a value of $X_{\text{CO}} = 2 \times 10^{20} \text{ cm}^{-2} (\text{K km s}^{-1})^{-1}$ measured in the Milky

Way, following previous studies (Olivares et al. 2019; Russell et al. 2019; Fujita et al. 2023; Fujita et al. 2024 and see their discussion). From these values we found $M_{\text{mol}} = (9.5 \pm 5.5) \times 10^6 M_{\odot}$.

3 Model description

If protons are accelerated in the AGN at the center of NGC 4278 and subsequently escape, they can interact with the surrounding molecular cloud and emit gamma rays and neutrinos by pp interactions. We discuss the gamma-ray emission based on a model constructed previously in the context of Sgr A* by Fujita et al. (2015) and Fujita et al. (2017).

3.1 CR acceleration in the RIAF

We assume that CR protons are accelerated in the RIAF. Following the stochastic acceleration model proposed by Kimura et al. (2015), we determine the spectrum of accelerated CRs. The typical energy of the accelerated CRs is calculated by equating their acceleration time in the RIAF to their escape time from the RIAF, which is approximately equal to their diffusion time (Kimura et al. 2015; Fujita et al. 2015). The energy is

$$\frac{E_{p,\text{eq}}}{m_p c^2} \sim 1.4 \times 10^5 \left(\frac{\dot{m}}{0.01} \right)^{1/2} \left(\frac{M_{\text{BH}}}{1 \times 10^7 M_{\odot}} \right)^{1/2} \left(\frac{\alpha}{0.1} \right)^{1/2} \times \left(\frac{\zeta}{0.1} \right)^3 \left(\frac{\beta}{3} \right)^{-2} \left(\frac{R_{\text{acc}}}{10 R_S} \right)^{-7/4}, \quad (2)$$

where m_p is the proton mass, $\dot{m} = \dot{M}/\dot{M}_{\text{Edd}}$ is the gas accretion rate normalized by the Eddington accretion rate, M_{BH} is the mass of the SMBH, α is the alpha parameter for the viscosity in the accretion flow (Shakura, & Sunyaev 1973), ζ is the ratio of the strength of the turbulent fields to that of the non-turbulent fields, β is the plasma beta parameter, R_{acc} is the typical radius where CRs are accelerated, and R_S is the Schwarzschild radius of the SMBH. The Eddington accretion rate is given by $\dot{M}_{\text{Edd}} = L_{\text{Edd}}/c^2$, where L_{Edd} is the Eddington luminosity. For NGC 4278 we set the black hole mass to $M_{\text{BH}} = 3.1 \times 10^8 M_{\odot}$ (Wang, & Zhang 2003; Chiaberge et al. 2005). In the fiducial model we set $\alpha = 0.1$, $\zeta = 0.05$, $\beta = 3$, and $R_{\text{acc}} = 10 R_S$, since the diffuse neutrino flux detected at energies of about 10–100 TeV by IceCube can be reproduced by the population of LLAGNs with these parameters (Kimura et al. 2015). We assume $\dot{m} = 5 \times 10^{-6}$ for the current Eddington ratio of NGC 4278 estimated from X-ray observations (Younes et al. 2010; Hernández-García et al. 2014). With these parameters we obtain $E_{p,\text{eq}} = 2.0 \text{ TeV}$. Note that we discuss the effects of varying \dot{m} , ζ and β later.

The luminosity of CRs accelerated in the RIAF is assumed to be $L_p = \eta_{\text{cr}} \dot{M} c^2$. We choose the parameter $\eta_{\text{cr}} = 0.015$ based on Kimura et al. (2015). Considering only stochastic acceleration, the production rate of protons in the momentum range p to $p + dp$ can be expressed as

$$\dot{N}(x) dx \propto x^{(7-3q)/2} K_{(b-1)/2}(x^{2-q}) dx, \quad (3)$$

where $x = p/p_{\text{cut}}$, K_ν is the Bessel function, and $b = 3/(2-q)$, and q represents the spectral index of the turbulent field (Becker et al. 2006). We set the lower bound of the CR momentum to $x = m_p c/p_{\text{cut}}$. We consider Kolmogorov-type turbulence, so the power-law index is $q = 5/3$. The cutoff momentum can be written as $p_{\text{cut}} = (2-q)^{1/(2-q)} p_{\text{eq}} = p_{\text{eq}}/27$, where $p_{\text{eq}} = E_{\text{eq}}/c$ (Becker et al. 2006; Kimura et al. 2015). We normalize equation (3) so that the total CR power is L_p .

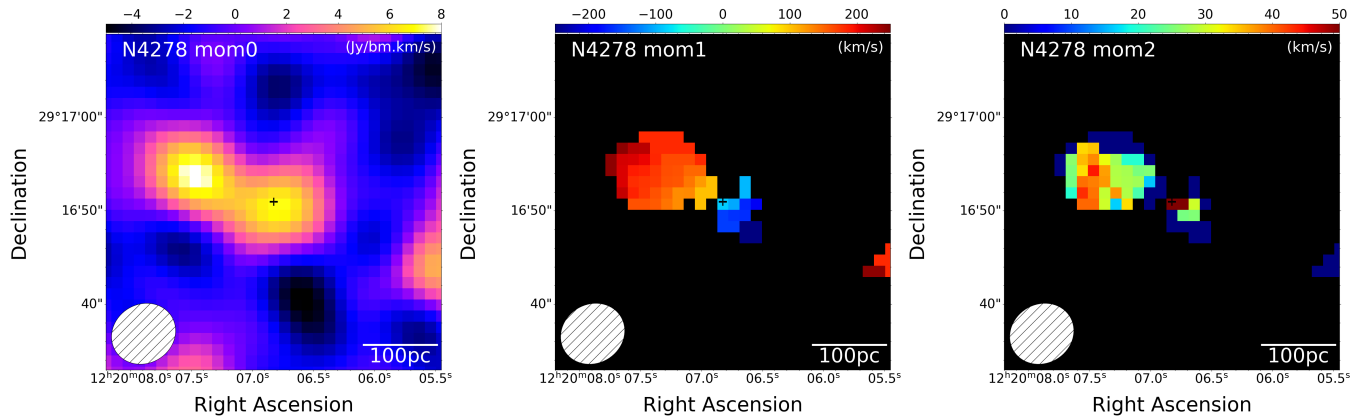


Fig. 1. CO emission from NGC 4278. From left to right: integrated intensity map (moment 0), velocity center distribution map (moment 1) of the $\geq 3\sigma$ CO emission, and velocity dispersion map (moment 2) of the $\geq 3\sigma$ CO emission. The position of the AGN is indicated by the cross. The beam size is shown in white at the bottom left of each panel. Alt text: Three color maps, each showing the intensity, velocity center and velocity dispersion of the CO emission.

3.2 Diffusion of CRs in the molecular cloud and gamma-ray emission

For simplicity, we assume that the system is spherically symmetric and that CR protons diffuse out from the central AGN into the surrounding molecular cloud. The cloud is uniform and has a radius of $R_{\text{mol}} = 100$ pc, the approximate apparent size of the actual cloud observed in NGC 4278 (figure 1 left). Its density is

$$\rho_{\text{mol}} = \frac{3M_{\text{mol}}}{4\pi R_{\text{mol}}^3} = 1.5 \times 10^{-22} \text{ g cm}^{-3} \left(\frac{M_{\text{mol}}}{9.5 \times 10^6 M_{\odot}} \right) \left(\frac{R_{\text{mol}}}{100 \text{ pc}} \right)^{-3}. \quad (4)$$

We solve the diffusion equation in spherical symmetry,

$$\frac{\partial f}{\partial t} = \frac{1}{r^2} \frac{\partial}{\partial r} \left(r^2 \kappa \frac{\partial f}{\partial r} \right) + Q \delta^3(\mathbf{r}), \quad (5)$$

where $f = f(t, r, p)$ is the distribution function of CR protons, t is time, r is the distance from the central AGN, p is the CR momentum, κ is the diffusion coefficient, $\delta^3(\mathbf{r})$ is the three-dimensional Dirac delta function, and Q is the CR source term written as $\int 4\pi p^3 Q dp = L_p = \eta_{\text{cr}} \dot{M} c^2$. Since the cloud is very large compared to the size of the RIAF, we consider injection by a central point source. We assume that the system is in steady state, so that $\partial f / \partial t = 0$. Solving equation (5), we get

$$f = \frac{Q}{4\pi r \kappa}. \quad (6)$$

We assume that the diffusion coefficient of CRs in the molecular cloud is

$$\kappa(\chi, E_p, B) = 10^{28} \chi \left(\frac{E_p}{10 \text{ GeV}} \right)^{1/2} \left(\frac{B}{3 \mu\text{G}} \right)^{-1/2} \text{ cm}^2 \text{ s}^{-1}, \quad (7)$$

where χ is the reduction factor, E_p is the CR energy, and B is the magnetic field strength (Gabici et al. 2009). We assume $B = 1$ mG, which is consistent with the smaller values observed in molecular clouds near the Galactic Center (Guerra et al. 2023). Fiducially, we assume $\chi = 1$, which would be appropriate for the general interstellar medium (ISM), but not necessarily inside molecular clouds, particularly when a strong CR source is present (see below).

CR protons interact with protons in the molecular cloud and produce pions, which decay into gamma-ray photons, neutrinos, etc. We calculate the production rate of gamma rays and neutrinos using the code from Karlsson & Kamae (2008) and the parameterization of pp interactions by Kelner et al. (2006).

The pp interactions also act as an energy loss mechanism for the protons. The total inelastic cross section of the pp interaction is well approximated by

$$\sigma_{pp} = (34.3 + 1.88L + 0.25L^2) \left[1 - \left(\frac{E_{\text{th}}}{E_p} \right)^4 \right]^2 \text{ mb}, \quad (8)$$

where $E_{\text{th}} = 1.22$ GeV is the threshold energy for the production of π^0 mesons and $L = \ln(E_p/1 \text{ TeV})$ (Kelner et al. 2006). Thus, the total inelastic cross section at $E_p \sim 1$ TeV is $\sigma_{pp} \sim 3.4 \times 10^{-26} \text{ cm}^2$. Therefore, the pp cooling time of CRs at $E_p \sim 1$ TeV is

$$\begin{aligned} t_{pp} &\sim (n_{\text{mol}} \sigma_{pp} c K_{pp})^{-1} \\ &\sim 6.7 \times 10^5 \left(\frac{n_{\text{mol}}}{92 \text{ cm}^{-3}} \right)^{-1} \\ &\times \left(\frac{\sigma_{pp}}{3.4 \times 10^{-26} \text{ cm}^2} \right)^{-1} \left(\frac{K_{pp}}{0.5} \right)^{-1} \text{ yr}, \end{aligned} \quad (9)$$

where $n_{\text{mol}} = \rho_{\text{mol}}/m_p$ is evaluated from equation (4) and K_{pp} is the proton inelasticity. On the other hand, the diffusion time of CRs in the molecular cloud can be estimated as

$$\begin{aligned} t_{\text{diff}} &= \frac{R_{\text{mol}}^2}{6\kappa} \\ &\sim 9.2 \times 10^4 \chi^{-1} \left(\frac{R_{\text{mol}}}{100 \text{ pc}} \right)^2 \\ &\times \left(\frac{E_p}{1 \text{ TeV}} \right)^{-1/2} \left(\frac{B}{1 \text{ mG}} \right)^{1/2} \text{ yr}, \end{aligned} \quad (10)$$

using equation (7). Since t_{pp} is longer than t_{diff} for $\chi = 1$ at the typical energy of the CRs ($E_p \sim 1$ TeV), we neglect the effect of pp cooling in equations (5) and (6) for the fiducial case ($\chi = 1$).

We note that the observed increase in the gamma-ray luminosity of NGC 4278 (Cao et al. 2024b) over a period of ~ 100 days cannot be explained by our model because this duration is much shorter than the CR diffusion timescale given in equation (10). The increase may instead be related to the activity of the jet (Cao et al. 2024b). Explanation of the variable gamma-ray component is outside the scope of this paper.

4 Results

4.1 Fiducial model

Figure 2 shows the model spectra of gamma-ray emission from the molecular cloud for the fiducial case ($\dot{m} = 5 \times 10^{-6}$, $\chi = 1$,

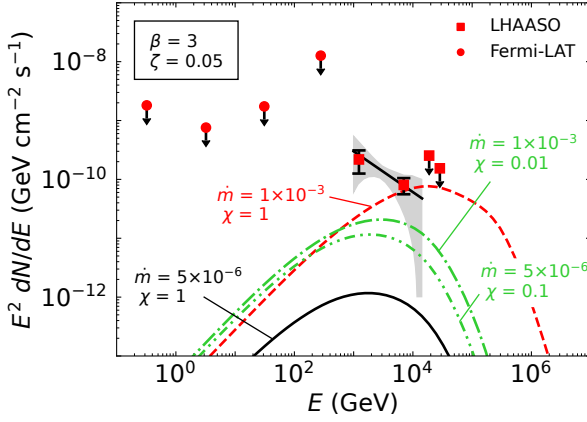


Fig. 2. Spectra of the hadronic gamma-ray emission model from the molecular cloud in NGC 4278 for $\dot{m} = 5 \times 10^{-6}$ and $\chi = 1$ (black solid), $\dot{m} = 1 \times 10^{-3}$ and $\chi = 1$ (red dashed), $\dot{m} = 5 \times 10^{-6}$ and $\chi = 0.1$ (green dot-dashed), and $\dot{m} = 5 \times 10^{-6}$ and $\chi = 0.01$ (green dot-dot-dashed) when $\beta = 3$ and $\zeta = 0.05$. Filled squares and circles show the data from LHAASO (Cao et al. 2024b) and Fermi (Wang et al. 2024), respectively. Alt text: Line graph. The x axis shows the photon energy from 10^{-1} to 10^7 giga electron volts. The y axis shows the energy flux from 10^{-13} to 10^{-7} giga electron volts per squared centimeter per second.

$\zeta = 0.05$, and $\beta = 3$), compared with the observed data from LHAASO (Cao et al. 2024b) and Fermi (Wang et al. 2024). Since gamma-ray attenuation due to pair production with the extragalactic background light (EBL) can be effective for VHE gamma rays, the effect is included in the LHAASO data using the EBL model of Saldana-Lopez et al. (2021). Figure 2 shows that the fiducial model (black solid curve) significantly falls short of the observations.

4.2 Enhanced past activity and CR confinement

Considering the simplicity of our model and the large uncertainties expected in some of the parameters, we vary them from the fiducial values to see if the model can be made consistent with the observations.

First, we explore the possibility of a larger \dot{m} . The AGN at the center of the Milky Way, Sgr A*, is also a LLAGN. Its current mass accretion rate is $\dot{m} = 4.2 \times 10^{-6}$ (Fujita et al. 2015), similar to that of NGC 4278 ($\dot{m} \sim 5 \times 10^{-6}$; Younes et al. 2010; Hernández-García et al. 2014). However, previous studies suggest that \dot{m} of Sgr A* was 10^3 – 10^4 times larger at epochs more than 100 years ago (Koyama et al. 1996; Totani 2006; Ryu et al. 2013). Fujita et al. (2015) showed that the gamma-ray emission observed from the molecular clouds around Sgr A* can be explained if the increased CR production associated with the past enhanced activity is taken into account.

For NGC 4278, X-ray observations over the last 20 years reveal periods when the X-ray flux was about an order of magnitude higher, plausibly due to a correspondingly higher \dot{m} , compared to later epochs when $\dot{m} \sim 5 \times 10^{-6}$ was inferred (Lian et al. 2024). It is possible that \dot{m} was even higher on longer timescales in the past, which may possibly be related to the presence of massive molecular and HI gases. Thus, we consider the case where the AGN activity and CR production of NGC 4278 was much higher in the past and has recently become more quiet. As long as the quiescent period is shorter than the CR diffusion time, $t_{\text{diff}} \sim 10^5$ yr (equation (10)), the current gamma-ray flux from the molecular cloud is

relatively insensitive to the recent decrease in CR production.

The gamma-ray emission for the case of $\dot{m} = 1 \times 10^{-3}$ with other parameters remaining fiducial is shown by the red dashed curve in figure 2. Compared to the fiducial case (black solid curve), the flux around $E \approx 10$ TeV is increased significantly. However, according to equation (2), larger \dot{m} results in larger typical CR energy $E_{p,\text{eq}}$, and the peak of the gamma-ray spectrum is shifted toward higher energies; for $\dot{m} = 1 \times 10^{-3}$, $E_{p,\text{eq}} = 29$ TeV (equation (2)). This model is not compatible with the observed LHAASO spectrum at $E = 1 - 10$ TeV.

Second, we consider the possibility of a smaller diffusion coefficient inside the molecular cloud, since the nature of the relevant magnetic turbulence that govern CR propagation is uncertain and in principle can be very different from the general ISM, especially near a strong CR source. Various observations indicate that the diffusion coefficient in the vicinity of potential CR sources could be one to two orders of magnitude smaller than the value inferred for the Milky Way ISM, such as in the Cygnus bubble (LHAASO Collaboration 2024a; Nie et al. 2024), around the microquasar SS 433 (LHAASO Collaboration 2024b), and in the pulsar TeV halos (Abeysekara et al. 2017; Bao et al. 2022). The magnetohydrodynamical waves self-generated by the CRs escaping from the source could be the origin of the small diffusion coefficient (Fujita et al. 2009; Fujita et al. 2010; Schroer et al. 2022). Therefore, we reduce the coefficient from $\chi = 1$ in equation (7), keeping the other parameters fiducial. Note that the dependence on χ and B is degenerate in equation (7), and the results are identical for given $\chi B^{-1/2}$. A smaller χ implies a longer t_{diff} (equation (10)), which could exceed t_{pp} (equation (9)). For simplicity, we include the effect of pp cooling by ignoring the CRs at $r > R_{\text{cool}}$, where R_{cool} is the cooling radius at which $t_{pp} = t_{\text{diff}}$. Specifically, equation (6) is changed to

$$f = \begin{cases} \frac{Q}{4\pi r \kappa(\chi, E_p, B)} & \text{if } r < R_{\text{cool}}, \\ 0 & \text{if } r \geq R_{\text{cool}}, \end{cases} \quad (11)$$

$$R_{\text{cool}} = \sqrt{6\kappa t_{pp}}. \quad (12)$$

Figure 2 shows the gamma-ray spectra for $\chi = 1$ (black solid curve), 0.1 (green dot-dashed curve), and 0.01 (green dot-dot-dashed curve). Comparing the cases of $\chi = 1$ and 0.1, a smaller χ results in a larger gamma-ray flux for this range of χ . Since we assume that ρ_{mol} is constant at $r < R_{\text{mol}}$, the gamma-ray flux at a given energy E saturates when $R_{\text{cool}} < R_{\text{mol}}$ for the CRs with $E_p \approx 10E$. Note that R_{cool} increases with E_p due to the energy dependence of κ (equations (7) and (12)). For our model with $\dot{m} = 5 \times 10^{-6}$, $\beta = 3$, $\zeta = 0.05$, the gamma-ray flux around $E = 1 - 10$ TeV saturates at $\chi \sim 0.01$. The maximal flux is about an order of magnitude lower than the observed values at $E \sim 10$ TeV. Thus, the reduced χ alone cannot explain the data.

Third, we modify the parameters related to the CR acceleration model explained in section 3.1. We focus on the plasma beta parameter β and the turbulence strength parameter ζ , as these are very uncertain theoretically as well as observationally, but can significantly affect the CR spectrum (equation (2)). Figure 3 shows the model gamma-ray flux when we vary β from 3 to 6, and ζ from 0.05 to 0.03, so that $E_{p,\text{eq}}$ is less than the fiducial value by a factor of 20. Note that $E_{p,\text{eq}} \propto \zeta^3 \beta^{-2}$ (equation (2)), so the dependence on ζ and β is degenerate. The typical CR energy is $E_{p,\text{eq}} = 0.11$ TeV for $\dot{m} = 5 \times 10^{-6}$, $E_{p,\text{eq}} = 0.38$ TeV for $\dot{m} = 6 \times 10^{-5}$, and $E_{p,\text{eq}} = 1.1$ TeV for $\dot{m} = 5 \times 10^{-4}$ (equation (2)). The observed gamma-ray flux at $E \sim 1 - 10$ TeV is well reproduced when $\dot{m} = 5 \times 10^{-4}$ and $\chi = 1$ (red dashed curve), or

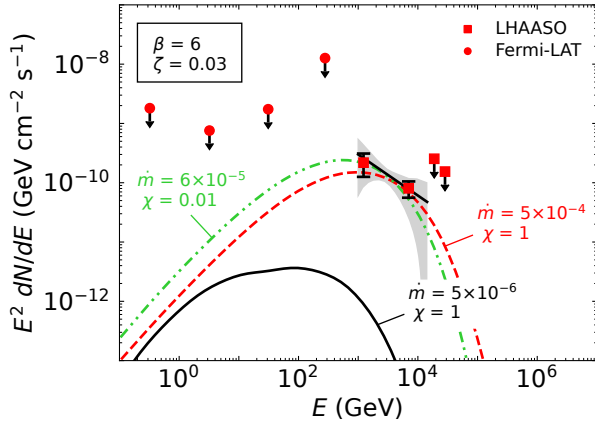


Fig. 3. Model gamma-ray spectra for $\dot{m} = 5 \times 10^{-6}$ and $\chi = 1$ (black solid), $\dot{m} = 5 \times 10^{-4}$ and $\chi = 1$ (red dashed), and $\dot{m} = 6 \times 10^{-5}$ and $\chi = 0.01$ (green dot-dashed) when $\beta = 6$, $\zeta = 0.03$. Otherwise similar to figure 2. Alt text: Line graph similar to figure 2.

$\dot{m} = 6 \times 10^{-5}$ and $\chi = 0.01$ (green dot-dashed curve). This suggests the existence of an allowed range of \dot{m} and χ for given β and ζ which determine $E_{p,eq}$ or the peak energy of the gamma-ray spectrum. Figure 5 shows the combination of \dot{m} and χ that can reproduce the observed spectrum when $\beta = 6$ and $\zeta = 0.03$. The range of $6 \times 10^{-5} \lesssim \dot{m} \lesssim 7 \times 10^{-4}$ is consistent with gamma-ray observations when $\chi < 1$ (dashed line). The value of \dot{m} indicates that the past activity of NGC 4278 may have been 10 to 100 times greater than at present ($\dot{m} = 5 \times 10^{-6}$).

4.3 HI gas

NGC 4278 is known to have an exceptionally large amount of HI gas for an elliptical galaxy, with total mass $\sim 10^8 M_\odot$ (Raimond et al. 1981; Morganti et al. 2006; Haynes et al. 2018). It appears as a spheroid with major and minor axes of ~ 37 kpc and ~ 30 kpc, respectively (Morganti et al. 2006). We calculate the contribution of the HI gas to the gamma-ray flux.

We set the HI gas mass to $M_{\text{HI}} = 3.5 \times 10^8 M_\odot$ (Haynes et al. 2018). We assume that it takes the form of a sphere with radius $R_{\text{HI}} \sim 15$ kpc. The mean density is

$$\begin{aligned} \rho_{\text{HI}} &= \frac{3M_{\text{mol}}}{4\pi R_{\text{HI}}^3} \\ &= 1.7 \times 10^{-27} \text{ g cm}^{-3} \left(\frac{M_{\text{HI}}}{3.5 \times 10^8 M_\odot} \right) \left(\frac{R_{\text{HI}}}{15 \text{ kpc}} \right)^{-3}. \end{aligned} \quad (13)$$

The effect of pp cooling on CRs in the HI gas can be estimated by equations (11) and (12) with κ (equation (7)) and t_{pp} (equation (9)) using parameters appropriate for the HI gas. We assume $B = 50 \mu\text{G}$ for the HI gas, which is similar to the values observed for intercloud regions around the Galactic Center of the Milky Way (Ferrière et al. 2011).

Figure 4 shows the result when $\dot{m} = 5 \times 10^{-4}$, $\chi = 1$, $\beta = 6$, and $\zeta = 0.03$. The contribution of the HI gas is less than 1/10 of that of the molecular cloud. Figure 5 shows the allowed combination of \dot{m} and χ . The range of $6 \times 10^{-5} \lesssim \dot{m} \lesssim 6 \times 10^{-4}$ is consistent with gamma-ray observations.

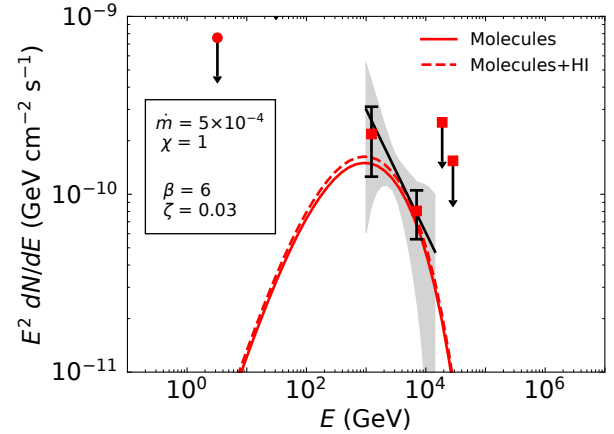


Fig. 4. Model gamma-ray spectra from the molecular cloud only (solid) and from both the molecular cloud and the HI gas (dashed) when $\dot{m} = 5 \times 10^{-4}$ and $\chi = 1$. Otherwise similar to figure 2. Alt text: Line graph similar to figure 2.

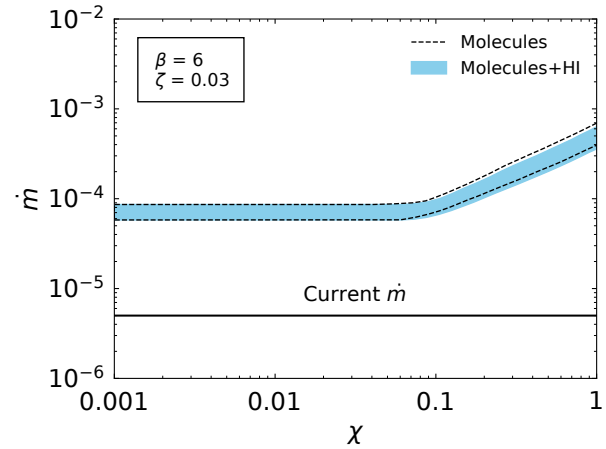


Fig. 5. The combination of \dot{m} and χ that can reproduce the observed gamma-ray data for the molecular cloud only (dashed) and for both the molecular cloud and the HI gas (cyan shaded region). The horizontal line represents the current accretion rate, $\dot{m} = 5 \times 10^{-6}$. Alt text: Graph of the parameter space. The x axis shows χ from 0.001 to 1. The y axis shows \dot{m} from 10^{-6} to 10^{-2} .

4.4 Neutrino emission

The detection of high-energy neutrinos would strongly support our hadronic model. In figure 6, the blue curve shows the predicted neutrino flux when $\dot{m} = 5 \times 10^{-4}$, $\chi = 1$, $\beta = 6$, and $\zeta = 0.03$, corresponding to the gamma-ray emission model shown as the dashed curve in figure 4. The figure also shows the detectability of neutrinos for the declination of NGC 4278 with IceCube and IceCube-Gen2, in terms of the differential point source sensitivity at 90% CL and 5σ discovery potential (The IceCube-Gen2 Collaboration 2021). The sensitivity at 90% confidence level (CL) is defined as the neutrino flux required for the test statistic (TS) distribution to exceed the median of the background-only TS distribution 90% of the time. The 5σ discovery potential is defined as the neutrino flux required for the TS to exceed the 5σ fluctuation of the background-only TS distribution 50% of the time (Alfaro et al. 2024). The assumed declination is $\delta = 30^\circ$, close to that of NGC 4278 ($\delta \sim 29.28^\circ$; Xu et al. 2019). The predicted neutrino flux is much lower than the sensitivity of IceCube-Gen2. Therefore,

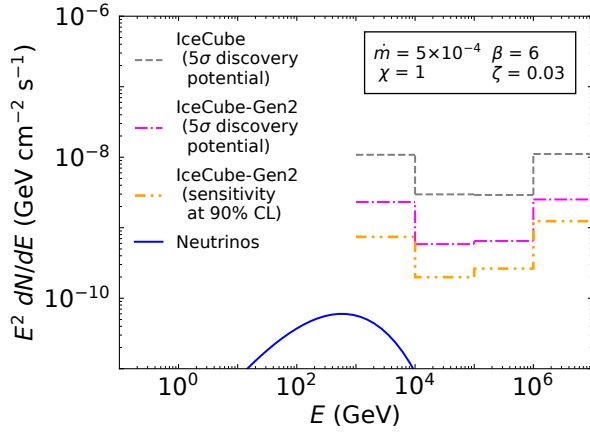


Fig. 6. The neutrino flux from the molecular cloud and the HI gas when $\dot{m} = 5 \times 10^{-4}$ and $\chi = 1$. The differential sensitivities for the detection of point sources (5σ discovery potential and sensitivity at 90% CL) of IceCube and IceCube-Gen2 are also shown for the declination $\delta = 30^\circ$ (The IceCube-Gen2 Collaboration 2021). Alt text: Line graph.

neutrino detection will be difficult in the near future.

5 Conclusions

We have investigated the origin of the very high-energy gamma rays from NGC 4278 detected by LHAASO. First, we analyzed ALMA data and found that the galaxy has a massive ($\sim 10^7 M_\odot$) molecular cloud within a few 100 pc from its center. Then we constructed a theoretical model in which CR protons are stochastically accelerated in a RIAF around the central SMBH with power proportional to the accretion rate. The CRs escaping from the RIAF enter the surrounding molecular cloud and produce gamma rays and neutrinos through pp interactions.

We calculated the gamma-ray flux from the molecular cloud and found that it falls short of that observed by LHAASO if the accretion rate onto the SMBH has persisted at the currently estimated rate over timescales of 10^5 yr relevant for CR diffusion. Therefore, we considered models with an enhanced past accretion rate and a suppressed diffusion coefficient for CR transport. The former is motivated by observations of Sgr A*, an LLAGN known to have had significantly higher past activity, as well as past X-ray observations of NGC 4278. The latter can be realized if the turbulence inside the molecular cloud is stronger than in the general ISM, possibly generated by the escaping CRs themselves. We showed that the observed gamma-ray flux can be reproduced if the accretion rate was ~ 10 – 100 times higher in the past and the diffusion coefficient is $\lesssim 0.1$ – 1 times smaller than the value inferred for the ISM.

We also calculated the gamma rays from the HI gas outside the molecular cloud of NGC 4278 and found that its contribution are much smaller than that of the molecular cloud. We also found that the pp neutrinos co-produced with the gamma rays from the molecular cloud and the HI gas of NGC 4278 are unlikely to be observable even with the future neutrino observatory IceCube-Gen2.

Acknowledgments

This work was supported by NAOJ ALMA Scientific Research grant Code 2022-21A, and JSPS KAKENHI Grant Nos.

JP22H01268, JP22H00158, JP22K03624, JP23H04899 (Y.F.); JP22K03686, JP25K01045 (N.K.); JP23H04896 (S.I). This paper makes use of the ALMA data: ADS/JAO.ALMA#2022.1.01173.S. ALMA is a partnership of ESO (representing its member states), NSF (USA) and NINS (Japan), together with NRC (Canada), MOST and ASIAA (Taiwan), and KASI (Republic of Korea), in cooperation with the Republic of Chile. The JAO is operated by ESO, AUI/NRAO and NAOJ. Data analysis was in part carried out on the Multi-wavelength Data Analysis System operated by the Astronomy Data Center (ADC), National Astronomical Observatory of Japan.

References

- Abeyskara, A. U., Albert, A., Alfaro, R., et al. 2017, *Science*, 358, 911 doi:10.1126/science.aan4880
- Abdollahi, S., Acero, F., Baldini, L., et al. 2022, *ApJS*, 260, 53 doi:10.3847/1538-4365/ac6751
- Alfaro, R., Alvarez, C., Arteaga-Velázquez, J. C., et al. 2024, *ApJ*, 976, 8 doi:10.3847/1538-4357/ad812f
- Ballet, J., Bruel, P., Burnett, T. H., Lott, B., & The Fermi-LAT collaboration. 2023, arXiv e-prints, arXiv:2307.12546 doi:10.48550/arXiv.2307.12546
- Bao, L.-Z., Fang, K., Bi, X.-J., & Wang, S.-H. 2022, *ApJ*, 936, 183 doi:10.3847/1538-4357/ac8b8a
- Becker, P. A., Le, T., & Dermer, C. D. 2006, *ApJ*, 647, 539 doi:10.1086/505319
- Bolatto, A. D., Wolfire, M., & Leroy, A. K. 2013, *ARA&A*, 51, 207 doi:10.1146/annurev-astro-082812-140944
- Bronzini, E., Grandi, P., Torresi, E., & Buson, S. 2024, *ApJ*, 977, 16 doi:10.3847/2041-8213/ad93cf
- Cao, Z., Aharonian, F., An, Q., et al. 2024a, *ApJS*, 271, 25 doi:10.3847/1538-4365/acfd29
- Cao, Z., Aharonian, F., An, Q., et al. 2024b, *ApJ*, 971, 45 doi:10.3847/2041-8213/ad5e6d
- Chiaberge, M., Capetti, A., & Macchetto, F. D. 2005, *ApJ*, 625, 716 doi:10.1086/429612
- Combes, F., Young, L. M., & Bureau, M. 2007, *MNRAS*, 377, 1795 doi:10.1111/j.1365-2966.2007.11759.x
- Dutta, S., & Gupta, N. 2024, *ApJ*, 974, 56 doi:10.3847/1538-4357/ad6d65
- Ferrière, K. 2011, in *IAU Symp. 271, Astrophysical Dynamics: From Stars to Galaxies*, ed. N. H. Brummell et al. (Cambridge: Cambridge Univ. Press), 170 doi:10.1017/S1743921311017583
- Fujita, Y., Izumi, T., Kawakatu, N., et al. 2023, *PASJ*, 75, 925. doi:10.1093/pasj/psad050
- Fujita, Y., Izumi, T., Nagai, H., et al. 2024, *ApJ*, 964, 29. doi:10.3847/1538-4357/ad28c0
- Fujita, Y., Kimura, S. S., & Murase, K. 2015, *Phys. Rev. D*, 92, 023001 doi:10.1103/PhysRevD.92.023001
- Fujita, Y., Murase, K., & Kimura, S. S. 2017, *J. Cosmol. Astropart. Phys.*, 04, 037 doi:10.1088/1475-7516/2017/04/037
- Fujita, Y., Ohira, Y., & Takahara, F. 2010, *ApJL*, 712, L153. doi:10.1088/2041-8205/712/2/L153
- Fujita, Y., Ohira, Y., Tanaka, S. J., et al. 2009, *ApJL*, 707, L179. doi:10.1088/0004-637X/707/2/L179
- Gabici, S., Aharonian, F. A., & Casanova, S. 2009, *MNRAS*, 396, 1629 doi:10.1111/j.1365-2966.2009.14832.x
- Giroletti, M., Taylor, G. B., & Giovannini, G. 2005, *ApJ*, 622, 178 doi:10.1086/427898
- González-Martín, O., Masegosa, J., Márquez, I., Guainazzi, M., & Jiménez-Bailón, E. 2009, *A&A*, 506, 1107 doi:10.1051/0004-6361/200912288
- Guerra, J. A., Lopez-Rodriguez, E., Chuss, D. T., Butterfield, N. O., & Schmelz, J. T. 2023, *ApJ*, 166, 37 doi:10.3847/1538-3881/acdadcd
- Haynes, M. P., Giovanelli, R., Kent, B. R., et al. 2018, *ApJ*, 861, 49 doi:10.3847/1538-4357/aac956
- Hernández-García, L., González-Martín, O., Masegosa, J., & Márquez, I. 2014, *A&A*, 569, 26 doi:10.1051/0004-6361/201424140

- Ho, L. C., Filippenko, A. V., & Sargent, W. L. W. 1997, *ApJS*, 112, 315
doi:10.1086/313041
- Ho, L. C. 2008, *A&A*, 46, 475 doi:10.1146/annurev.astro.45.051806.110546
- Karlsson, N., & Kamae, T. 2008, *ApJ*, 674, 278 doi:10.1086/524353
- Kelner, S. R., Aharonian, F. A., & Bugayov, V. V. 2006, *Phys. Rev. D*, 74, 034018 doi:10.1103/PhysRevD.74.034018
- Kimura, S. S., Murase, K., & Toma, K. 2015, *ApJ*, 806, 159
doi:10.1088/0004-637X/806/2/159
- Koyama, K., Maeda, Y., Sonobe, T., et al. 1996, *PASJ*, 48, 249
doi:10.1093/pasj/48.2.249
- LHAASO Collaboration 2024a, *Sci. Bull.*, 69, 449
doi:10.1016/j.scib.2023.12.040
- LHAASO Collaboration 2024b, arXiv e-prints, arXiv:2410.08988
doi:10.48550/arXiv.2410.08988
- Lian, J.-S., Li, J.-X., Hu, X.-K., Gan, Y.-Y., Wu, T.-Z., & Zhang, J. 2024, *ApJ*, 974, 134 doi:10.3847/1538-4357/ad6e81
- Morganti, R., de Zeeuw, P. T., Oosterloo, T. A., et al. 2006, *MNRAS*, 371, 157 doi:10.1111/j.1365-2966.2006.10681.x
- McMullin, J. P., Waters, B., Schiebel, D., et al. 2007, *Astronomical Data Analysis Software and Systems XVI*, 376, 127
- Nie, L., Qian, X.-L., Guo, Y.-Q., & Liu, S.-M. 2024, *ApJ*, 974, 276
doi:10.3847/1538-4357/ad7eab
- Olivares, V., Salome, P., Combes, F., et al. 2019, *A&A*, 631, A22
doi:10.1051/0004-6361/201935350
- Raimond, E., Faber, S. M., Gallagher, J. S., III, & Knapp, G. R. 1981, *ApJ*, 246, 708 doi:10.1086/158967
- Rose, T., Edge, A. C., Combes, F., et al. 2019, *MNRAS*, 485, 229
doi:10.1093/mnras/stz406
- Russell, H. R., McNamara, B. R., Fabian, A. C., et al. 2019, *MNRAS*, 490, 3025 doi:10.1093/mnras/stz2719
- Ryu, S. G., Nobukawa, M., Nakashima, S., Tsuru, T. G., Koyama, K., & Uchiyama, H. 2013, *PASJ*, 65, 33 doi:10.1093/pasj/65.2.33
- Saldana-Lopez, A., Domínguez, A., Pérez-González, P. G., Finke, J., Ajello, M., Primack, J. R., Paliya, V. S., & Desai, A. 2021, *MNRAS*, 507, 5144
doi:10.1093/mnras/stab2393
- Shakura, N. I., & Sunyaev, R. A. 1973, *A&A*, 24, 337
- Schroer, B., Pezzi, O., Caprioli, D., Haggerty, C. C., & Blasi, P. 2022, *MNRAS*, 512, 233 doi:10.1093/mnras/stac466
- The IceCube-Gen2 Collaboration 2021, *J.Phys.G*, 48, 6, 060501
doi:10.1088/1361-6471/abbd48
- Tonry, J. L., Dressler, A., Blakeslee, J. P., Ajhar, E. A., Fletcher, A. B., Luppino, G. A., Metzger, M. R., & Moore, C. B. 2001, *ApJ*, 546, 681
doi:10.1086/318301
- Totani, T. 2006, *PASJ*, 58, 965 doi:10.1093/pasj/58.6.965
- Wang, T. G., & Zhang, X. G. 2003, *MNRAS*, 340, 793 doi:10.1046/j.1365-8711.2003.06336.x
- Wang, Z. R., Xue, R., Xiong, D., et al. 2024, *ApJS*, 271, 10
doi:10.3847/1538-4365/ad168c
- Xu, M. H., Anderson, J. M., Heinkelmann, R., Lunz, S., Schuh, H., & Wang, G. L. 2019, *ApJS*, 242, 5 doi:10.3847/1538-4365/ab16ea
- Younes, G., Porquet, D., Sabra, B., Grosso, N., Reeves, J. N., & Allen, M. G. 2010, *A&A*, 517, 33 doi:10.1051/0004-6361/201014371
- Yuan, F., & Narayan, R. 2014, *ARA&A*, 52, 529 doi:10.1146/annurev-astro-082812-141003